Three-dimensional segmentation and symbolic representation of cerebral vessels on 3DRA images of arteriovenous malformations

Y. Chenoune, O. Tankyevych, F. Li, M. Piotin, R. Blanc, E. Petit

Version of Record: https://www.sciencedirect.com/science/article/pii/S0010482519303579
Manuscript_c4e06c5e006d20d0709fc4dabc5d3c8c

Three-Dimensional Segmentation and Symbolic Representation of Cerebral Vessels on 3DRA Images of Arteriovenous Malformations

Y. Chenoune[1,2], O. Tankyevych[2], F. Li[1], M. Piotin[3], R. Blanc[3], E. Petit[2]

[1]ESME Sudria Research Lab, Paris, France

[2]Université Paris-Est, LISSI (EA 3956), UPEC, F-94010, Vitry-sur-Seine, France

[3]Fondation Ophtalmologique de Rothschild, Interventional Neuroradiology Department, Paris, France

Abstract

Background: Endovascular embolization is a minimally invasive interventional method for the treatment of neurovascular pathologies such as aneurysms, arterial stenosis or arteriovenous malformations (AVMs). In this context, neuroradiologists need efficient tools for interventional planning and microcatheter embolization procedures optimization. Thus, the development of helpful methods is necessary to solve this challenging issue.

Methods: A complete pipeline aiming to assist neuroradiologists in the visualization, interpretation and exploitation of three-dimensional rotational angiographic (3DRA) images for interventions planning in case of AVM is proposed. The developed method consists of two steps. First, an automated 3D region-based segmentation of the cerebral vessels which feed and drain the AVM is performed. From this, a graph-like tree representation of these connected vessels is then built. This symbolic representation provides a vascular network modelization with hierarchical and geometrical features that helps in the understanding of the complex architecture of the AVM.

Results: The developed workflow achieves the segmentation of the vessels and of the malformation. It improves the 3D visualization of this complex network and highlights its three main components that are the arteries, the veins and the nidus. The symbolic representation then brings a better comprehension of the vessels angioarchitecture. It provides decomposition into topologically related vessels, offering the possibility to reduce the complexity due to the malformed vessels and also determine the optimal paths for AVM embolization during interventions planning.

Conclusions: A relevant vascular network modelization has been developed that constitutes a breakthrough in the assistance of neuroradiologists for AVM endovascular embolization planning.

Index Terms- 3D Vascular Segmentation; Symbolic Representation; 3DRA; Interventional Planning; Cerebral Arteriovenous Malformation; Vascular Network.

E-mail addresses

Yasmina Chenoune (PhD, corresponding author: yasmina.chenoune@esme.fr) and Fan Li (PhD, lifan9880@163.com) are with the ESME Research Lab, 40 rue du docteur Roux, 75015, Paris, France.

Doctor Raphaël Blanc (rblanc@for.paris) and Professor Michel Piotin (mpiotin@fo-rothschild.fr) are with the Fondation Ophtalmologique Adolphe de Rothschild, Interventional Neuroradiology Department, 29 Rue Manin, 75019, Paris, France.

Olena Tankyevych (PhD, olena.tankyevych@u-pec.fr) and Professor Eric Petit (eric.petit@u-pec.fr) are with the Laboratoire Images, Signaux et Systèmes Intelligents, 120 Rue Paul Armangot, 94400 Vitry-sur-Seine, France.

1. INTRODUCTION

1.1 Background and purpose

The segmentation of vascular structures is essential in diagnosis and clinical analysis of cerebral vascular pathologies. This segmentation is a necessary preliminary step in the three-dimensional (3D) structural and functional modelling of vessels, which is of significant interest for the preoperative planning of endovascular treatment. A 3D representation of the cerebral vascular network may also help decision-making during microcatheter embolization procedures because it improves the visualization of the vessels which have various shapes and sizes. The presence of pathology such as arteriovenous malformation (AVM) introduces an additional difficulty, due to the tangle of the malformed vessels. Dedicated tools are so needed to facilitate analysing and interpreting these complex vascular networks.

1.2 Cerebral AVM diagnosis and treatment

Cerebral AVM results from abnormal connections between arteries and veins through a direct shunt localized into a so called “nidus” structure which replaces the capillary network. This direct connection increases the blood pressure in the brain and the risk of breakage and haemorrhage [1]. These congenital lesions are often incidentally detected by computed tomography angiography (CTA) or magnetic resonance angiography (MRA) dictated for headaches or seizures. Imaging is therefore of great importance for the diagnosis and the characterization of the angioarchitecture and the treatment of these malformations [2] which present multiple feeding arteries, enlarged draining veins and an important tangle of vessels forming the nidus. The recommended treatment option for these malformations can be microsurgical resection, stereotactic radiotherapy or endovascular embolization. Each of these options has its own advantages and limitations and combined approaches are often used in practice. Endovascular approach is considered a mini-invasive technique as it does not require opening of the skull base as conventional neurosurgery. It allows control deposition of embolic agent but requires X-Rays exposure. Radiosurgery, does not require skull opening but is limited to small or mid-size AVM and the delay to induce cure of the lesion by vascular sclerosis is about 2 to 3 years, a period of time during which an haemorrhage can occur. Surgery is considered the standard of cure as it allows for definitive resection of the malformation but requires a craniotomy and cannot reach lesions located deeply in the brain. All those reasons make the combination of the techniques (multimodal approach) a preferred choice nowadays [3].

1.3 Endovascular embolization planning

Among the previously cited therapeutic options, endovascular embolization is an efficient treatment therapy and a good alternative to open surgery. It consists of navigating with microcatheters from the groin throughout the intracranial vasculature and injecting a glue-like material to obstruct the blood supplies to the malformation. As for diagnosis, imaging plays a major role in the pre- and perioperative phases of the endovascular treatment. Conventional 2D digital subtraction angiography (DSA) has long been considered as the gold standard for the detection of aneurysms and AVMs [4]. However, this imaging technique presents some limitations such as repeated injections of contrast agent and high radiation dose. In the last few years, 3D rotational angiography (3DRA) imaging became a standard in endovascular therapy interventions. Currently, this imaging technique provides 3D high-resolution images of the vessels, allowing an accurate analysis of the arterial supply of AVMs. Nevertheless, in practice, these two imaging modalities remain insufficient for the visual tracking and manipulation of vessels paths. 3DRA being currently the most accurate imaging device for AVMs, we aimed to perform the 3D modelization of the vessels on these images.

1.4 Vascular structures segmentation

As previously mentioned, the 3D representation of the cerebral vascular structures requires their prior segmentation. Numerous difficulties must be taken into account such as the variability of vessels size and shape, the multiple branches and crossings of the network, as well as noise and pixels intensity heterogeneity on the images. This is a widely addressed issue and different approaches were used depending on imaging modality, considering anatomical structure or application fields. Several works in the literature were dedicated to vessels extraction methods. Kirbas and Quek [5] proposed to classify them into six categories: pattern recognition techniques, model-based approaches, tracking-based approaches, artificial intelligence, neural networks and tube-like objects determination. Lesage et al. [6] discussed the segmentation of angiographic images from three aspects: the vessel models, the vessel-specific features and the extraction schemes. Both reviews focused on the segmentation methods regardless of applications (cerebral, retinal, cardiac, pulmonary, etc.) or modalities (DSA, MRA, CTA, 2D, 3D etc.).

In this paper, we focus on the segmentation of cerebral vascular network. Among the different proposed approaches, multiscale model-based techniques using tubular or cylindrical models were

applied to X-ray and MRA images [7] and to MRI and MRA images [8]. Statistical mixture models relying on the analysis of pixels intensity distribution have been also widely used. Some authors proposed to apply these models on 3DRA images based on maximum intensity projection (MIP) [9], on Phase Contrast-MRA [10] and TOF-MRA images [11]. Other works focused on pixel-based thresholding procedures where a local optimal threshold is calculated for segmenting and reconstructing cerebral vessels from MRA [12]. In more recent works, a thresholding segmentation algorithm was applied on MRA [13] and a fully-automatic adaptive thresholding method successfully segmented 3D-DSA images [14]. To complete the grey level intensity information of the angiographic images, MIP images were also exploited to calculate the degree of membership of a voxel to extract the vasculature from MRA images [15].

In case of AVM, the challenge is to provide an accurate 3D visualization to distinguish the nidus from the feeding arteries and the draining veins. Another goal is to facilitate the interventions planning by the definition of the embolization paths. Some authors focused on the segmentation of nidus and connected vessels to the malformation. Bullit et al. [16] conducted very interesting works by exploiting the parent-child relationships of the vascular tree to semi-automatically extract the nidus from 3D-DSA and MRA images using a skeletonization algorithm. Babin et al. [17] used generalized morphological profiles [18] carried out by varying differential structuring elements (SE). These SE are especially adapted for different vessels contrast and sizes for AVM segmentation on 3D-CTA images. The arteries and veins were identified by their radius and separated from the nidus. More recently, they proposed a graph-based method for the draining veins extraction on 3DRA images [19]. Hsu et al. presented a fully automated vessel enhancement pipeline for multiple modalities such as 3DRA, MRA or CTA for generating anatomical network representations of the cerebral angioarchitecture [20].

1.5 Vascular network symbolic representation

Based on the segmentation step, a symbolic representation of the vascular network has to be performed to modelize its complex structure. Some works addressed the problem of generating such models on the basis of medical imaging datasets [21]. The model must bring global information on the network: mainly its topology but also mechanical properties as for instance flow or pressure measurements. Local features such as diameter, length or tortuosity of vessels can also enrich this model.

The symbolic representation gives clinicians a deep and accurate understanding of complex angioarchitectures [22].

Bullitt et al. [16] first introduced the notion of symbolic representation for the 3D analysis of the intracerebral vascular network. They described the minimum spanning tree algorithm to produce directed graphs of the intracerebral vasculature from segmented MRA data. From selected seed points, the tree structure was created by progressively linking segmentation points that satisfy both distance and intensity conditions. Later, Bullitt et al. [23] applied this algorithm on MRA images to segment the MAV. The nidus was interactively or automatically extracted. The results provided new visualizations and highlighted the relationships between the nidus and the feeding and draining vessels in the 3D space. One of the limitations of this methodology was that a processing time of 1-2 hours was required.

Graß et al. proposed [24] to build a symbolic representation of vessel trees from 3DRA images. They assumed that the tree components can be separated into three hierarchical levels: generations, clusters, and voxels. This model was applied to determine contrast agent propagation and to calculate bolus arrival time (BAT) for AVM or aneurysm. More recently, other works have extended the symbolic representation approach to the study of graph and quantitative description. Sankowski et al. [25] focused on the estimations of vascular parameters: diameter, local direction, location of terminal points and bifurcation points. Some authors have studied the radius associated with each centre point [26], as well as the length of vessels [15]. Orlowski et al. [27] proposed a schematic representation of the AVM network where nidus, draining and supplying vessels are annotated with abbreviated symbols. However, the proposed diagram symbols and annotations do not express either the anatomical location of the AVM or the identities of the vessels to which it connects.

1.6 Clinical needs and objectives

In clinical routine and for embolization interventions planning, neuroradiologists determine the principal feeding arteries and draining veins of the AVM from 3DRA images. The optimal navigation paths of microcatheters are manually spotted on DSA images [2]. To deeply track the vessels and define embolization paths, clinicians need a new 3D representation allowing interactive model exploration. Clinical experiments require the possibility of 3D manipulation of the vascular network for the purpose of

tracking or isolating a specific vessel to study its trajectory, termination and connections with the other vessels.

In this paper, a complete processing pipeline for 3DRA images analysis is developed, aiming to 1) provide a relevant three-dimensional visualization of the vascular network, 2) elaborate an anatomical model of the cerebral vascular network and 3) define the embolization paths from the vascular network. The proposed 3D segmentation and symbolic representation methods are described in Section 2. The obtained results are then presented and discussed in section 3. Conclusions and perspectives are finally given in section 4.

2. MATERIAL AND METHODS

In this section, we present the 3DRA data acquisition protocol and the main steps of the proposed method to process these data: 1) pre-processing to automatically initiate the segmentation procedure, 2) 3D vascular structures segmentation and visualisation, 3) identification of arteries, veins and nidus and finally 4) symbolic representation of the vascular network and embolization paths extraction. The whole process is illustrated by a graphical algorithm on Figure 1.

2.1 Patients and 3DRA acquisitions

Ten patients (aged from 23 to 59 years, 7 men) underwent 3DRA exams. The acquisitions were performed with a Philips Allura angiographic unit (Philips Healthcare, the Netherlands) after 28 mL contrast agent injection to enhance the vessels, at 4 mL/second with a rotation of 210° and a delay of 3 seconds between injection and acquisition. Each obtained dataset was a 256x256x256 cubic matrix with a voxel size varying from 0.29 mm^3 to 0.49 mm^3. The 3D image was centred on the region of interest containing the AVM, the veins and the arteries connected to the nidus. The Xtravision (Philips Healthcare) angiographic unit delivers initial reconstructions of the vessels, used for the qualitative validation of our results. Besides, several cerebral angiogram acquisitions were performed by a biplane angiographic system (FD20/10, Philips Healthcare).

2.2 3D Region-growing-based vessels segmentation

The vascular network surrounding the AVM was segmented using a 3D region-growing-based algorithm. The basic approach is to start from selected seeds belonging to the structures to extract and to

grow by incrementally including neighbouring voxels according to pre-defined criteria. Thus the segmentation depends on two elements: the seeds initialization and the inclusion criteria.

2.2.1 Automatic seeds location

To initiate the region growing process, seeds points are automatically localized on the first slice of the 3DRA volume. The pixel intensity distribution of these images can be divided into two classes: vessels and background [9]. In order to obtain markers of the vessels, a thresholding using morphological geodesic reconstruction [28] is applied. Let I be a grayscale image and $Thres_{low}$ and $Thres_{high}$ two threshold values ($Thres_{low} < Thres_{high}$). The binary images resulting from the application of simple thresholdings using $Thres_{low}$ and $Thres_{high}$ values are, respectively named J and K.

Let $J_1, J_2, \dots J_n$ be the n connected components of J and $K_1, K_2, \dots K_m$ be the m connected components of K. Since it is easily proved that $K \subseteq J$, K is called marker and J is called mask. The reconstruction $R_{J(k)}$ of the mask J from a marker K is obtained by the union of the connected components of J which contains at least one common pixel with K:

$$\mathrm{R_{J(k)}} = \bigcup_{\mathrm{K}\cap \mathrm{J_i}\neq\emptyset} \mathrm{J_i} \tag{1}$$

Thus, the lower threshold $Thres_{low}$ allows separating the different regions while the upper threshold $Thres_{high}$ is used to mark the potential vessels. The centres of mass of the extracted regions are usually considered as the seed [29]. Nevertheless, when the borders of vessels are not convex, the centre of mass may be located outside the region [30]. To avoid this, we defined seed points called p_{centre} as follows:

$$\mathrm{p}_{centre} \in \underset{\mathrm{i}=1,\dots\mathrm{N}}{\mathrm{Argmin}}\, \mathrm{D}_{(\mathrm{p_i})} \tag{2}$$

with $D_{(pi)}$, a distance defined as the sum of the distances between the point p_i and all the other points p_j of a region of N pixels. This distance is expressed according to the respective coordinates (x_i, y_i) and (x_j, y_j) of p_i and p_j as follows:

$$\mathrm{D}_{(\mathrm{p_i})} = \sum_{\mathrm{j}=1}^{\mathrm{N}} \left(\left|\mathrm{x_i} - \mathrm{x_j}\right| + \left|\mathrm{y_i} - \mathrm{y_j}\right|\right) \tag{3}$$

Argmin represents the set of solutions of our minimization problem. Since we consider a finite set of elements, the minimization problem therefore admits at least one solution in this set. Since the solution exists, we are thus certain that the centre of mass of the vessel will be within the region

2.2.2 3D growing

Usually, for cerebral arterial network segmentation, the seed point is defined at the root of the vasculature tree where the Internal Carotid Artery (ICA) is the only visible vessel (see Fig 2.(a)). Thus, the segmentation automatically starts from this unique point on the first image of the 3DRA volume and grows until extracting the entire vessel with its branches. As mentioned in section 2.1, each 3DRA dataset was a cubic matrix with isotropic voxels. So, the evolution of the region growing algorithm is possible from one voxel to all its neighbours, in the three directions. The bifurcations are automatically detected as the region formed by the iterative inclusion of the voxels evolves in the three spatial directions.

2.2.3 Membership and stopping criterion

The membership criterion that controls the algorithm evolution is based on spatial proximity and homogeneity properties of adjacent pixels /voxels [31]. As 3DRA images present a good and uniform contrast between vascular structures and background, due to the injected contrast agent [32], the voxels intensity can be defined as a robust inclusion criterion.

Let I_{max} and I_{min} respectively denote the highest and the lowest intensity values in the whole volume. Let the voxel $p_i(x_i, y_i, z_i)$ be the initial seed point and $I(p_i)$ the intensity value of p_i. Each 6-connected neighbour p_j of p_i is labelled as the vessel including p_i if the following condition is satisfied:

$$\left|I(p_i) - I(p_j)\right| < T * |I_{max} - I_{min}| \quad (4)$$

with $I(p_j)$ the intensity of p_j and T a weighting parameter. If the condition (4) is verified for a neighbour voxel p_j of p_i, the voxel p_j is included in the segmented region and the process is iterated for its six neighbours. This process ends when no changes occur after two successive iterations.

2.3 Nidus, arteries and veins separation

One of the most challenging and complex tasks encountered by neuroradiologists is distinguishing the three main components that are feeding arteries, draining veins and nidus. Such visualization can help clinicians in understanding the angioarchitecture of AVMs. Few authors have addressed this issue. Forkert et al. [33], [34] proposed a fuzzy-based classification algorithm to perform vessel enhancement, automatic segmentation and structure separation from time-of-flight (TOF) MRA. Identification of

arteries and veins was performed by combining 4D information. Clarençon et al. [35] distinguished the three structures by manually tagging different vessels on 3DRA images and then propagated the labelled voxel with a region-growing-based algorithm. However, this algorithm is very time-consuming as it requires the tagging of 10 to 50 arteries or veins and a high calculation time.

In this work, we propose a morphological method to semi-automatically isolate the nidus from the connected arterial and venous vessels. Several assumptions are necessary to allow differentiating the nidus from the arteries and veins. First, we can consider that the nidus global form, in most cases is similar to a sphere. Secondly, due to the malformed vessels, it is the largest ball-like component obtained after the vascular network segmentation. So, a big spherical SE is first used to consecutively apply closing and opening operations on the segmented tree including the nidus. Multiple tests are required to define the appropriate sphere radius. This step allows approximately detecting the nidus. When removing the obtained “approximated nidus” from the initial segmented object, the vascular network is "broken" into two or more parts. To identify the arterial network from the venous one, a last admitted hypothesis is that among the obtained structures, the arterial network is the structure presenting the largest volume. Furthermore, as the region growing algorithm ensures the spatial continuity when evolving from the ICA, the arterial part of the network constitutes one single block.

2.4 Vessels symbolic representation

The segmentation of the 3DRA dataset leads to significant enhancement of the 2D or 3D local and global visualization, but it is also of great interest to derive a symbolic representation from the segmented vascular network to provide a better understanding of its complex angioarchitecture. In this work, the proposed symbolic representation model consists of a transformation from the segmented vascular network into a graph representing it with different topological and geometrical descriptors. To obtain this symbolic graph, our algorithm operates in three main steps: 1) skeletonization of the segmented vessels using an efficient parallel thinning algorithm; 2) identification of junction points (vertices) and vessel segments (edges) and 3) vascular network analysis via hierarchy schemes.

In the first step, a skeleton of the whole cerebral vasculature is constructed from the segmented object using the isthmus-based parallel and asymmetric 3D thinning algorithm [36]. A minimal representation of

the object with its topology preservation as well as its geometrical features is so obtained. This algorithm produces an asymmetric skeleton that is one pixel wide at all points except junctions. Moreover, this method aims to preserve the curves or more precisely, voxels that belong to 1D isthmuses, producing a curvilinear skeleton. To avoid topological holes, which create cycles in the skeleton, and prior to skeletonization, the segmented image is hole-closed using the algorithm described in [37]. This algorithm is based on some properties of the topological numbers and on the principle of the topological hull. One of its qualities is that it allows closing small 3D-holes, corresponding to noise while preserving relevant holes.

In the second step, the skeleton is separated into vessel segments defined as parts of the vascular tree delimited by two adjacent junction points [38]. Thus this representation is suitable for topological and quantitative analysis. This mapping of segments and junctions can be represented as a mathematical graph by associating each junction with a vertex and each segment with an edge in the graph. This process gives a correspondence between the graph segments and vessel skeleton branches and between skeleton branches and segmented vasculature. With the obtained skeleton and its graph, a hierarchy of vascular network is created using the Strahler Ordering method [39].

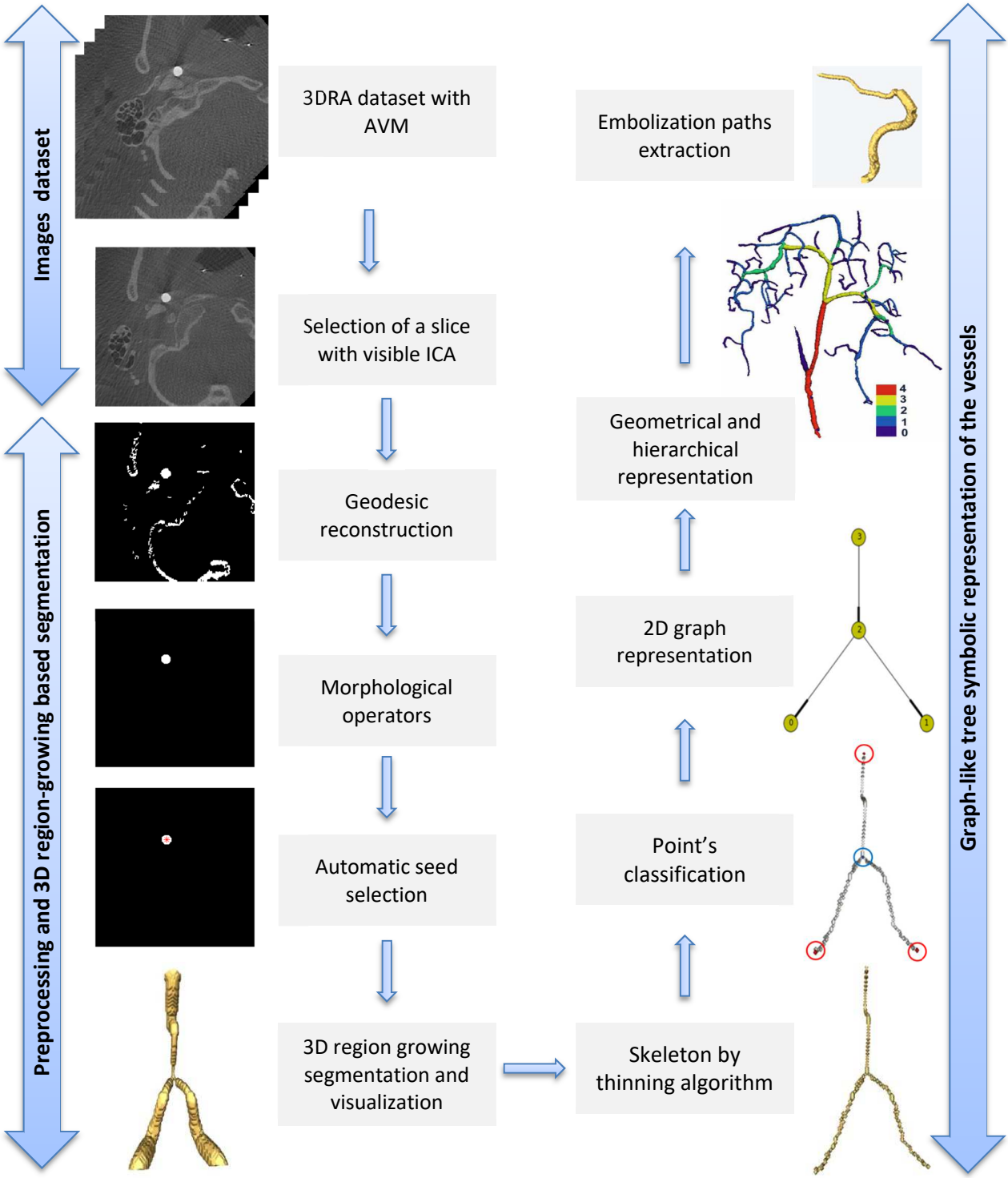

Fig 1. The graphical algorithm illustrating the whole process, including the 3D region-growing segmentation and the symbolic representation of the vessels

3. RESULTS AND DISCUSSION

3.1 3D region growing segmentation

The 3D vascular tree segmentation was achieved using a 3D region growing algorithm that evolves from the first slice of the 3D volume (Fig 2.(b)). The lower threshold $Thres_{low}$ and the upper threshold $Thres_{high}$ were respectively set to the normalized values 0.28 and 0.43. These values that allow defining the interval corresponding to the vascular structures were deduced from the logarithmic histogram of the 3DRA images [40]. The T weighting parameter (Equation 4) that achieves steady segmentations was experimentally set to 30±5% of segmented voxels on the whole volume. We observed that choosing the two thresholds and the weighting parameter values outside the defined intervals will result in an under- or an over-segmentation.

A unique seed point was automatically localized inside of the ICA which is the origin of the vasculature tree (Fig 2.(c)) whose diameter approximately varies between 3.5 and 4.5 mm in the skull. To only preserve the ICA, the remaining small structures were suppressed without difficulty using a morphological operator. Starting from this initial seed point, the 3D growing process is performed throughout the 3D volume to extract the entire vascular tree. In all cases and without any user interaction, the segmentation process achieves to detect the vascular network for different sizes and vessel shapes. Furthermore, the segmentation stage provides an automatic detection of the bifurcations points and extracts the small terminal branches even very fine ones (0.7 mm diameter).

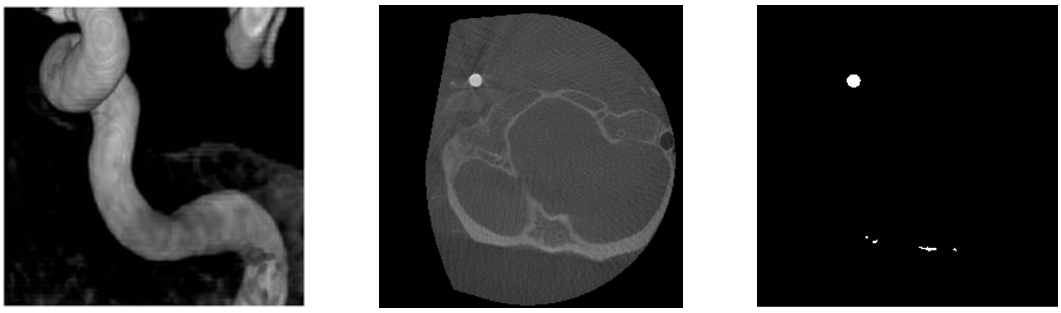

(a) (b) (c)

Fig 2. a) Region of interest on a 3DRA volume including the ICA, b) the first image of the corresponding stack of slices and c) initial binary shape used for positioning the seed point for region growing propagation.

The proposed segmentation algorithm presents the advantage of being automatically initialized. It's able to automatically segment a given vascular tree with its branches and detect the bifurcations as we can

see it on Figure 3. So, specific forms like malformed vessels and junctions are automatically managed. Moreover, the process depends on few parameters whose values adapt according to the image properties even for the detection of complex vascular structures.

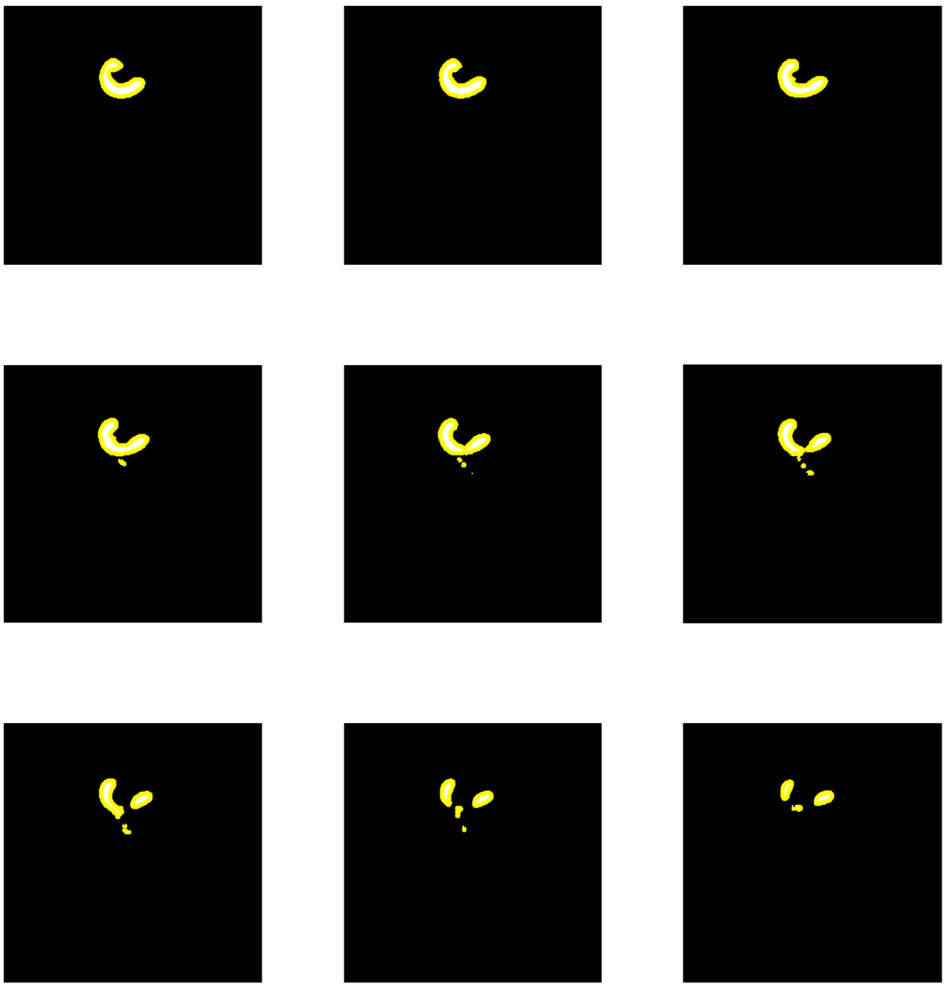

Fig 3. Illustration of region growing algorithm evolution with the automatic bifurcation points management.

3.2 Qualitative validation

The 3D vascular tree segmentation was performed on ten 3DRA datasets with AVMs. As previously mentioned in section 2.1, the 3D reconstructions delivered by the Xtravision Unit were considered as the reference for the qualitative validation of our results. This validation was independently performed by two neuroradiologists (RB and HR) and consisted of a visual comparison with volume rendering and 3D MIP rendering obtained with the imaging station.

The AMIRA 3D software (Thermo Fisher Scientific, Waltham, Massachusetts) was used to visualize our segmentation results. This tool allows showing different viewing angles for a greater visualization of

the vessels bifurcations. Figure 4 shows five examples with different AVMs of vascular networks segmentation, obtained from the 3DRA data. Fig 4.(a) shows an angle of visualization with the AMIRA 3D software of the results obtained by our method. Figs 4.(b) and 4.(c) represent the visualization using the Osirix open-source software (Pixmeo SARL, Geneva, Switzerland) respectively of the corresponding volume and 3D MIP rendering proposed by the Xtravision Unit.

Therefore the experts visually analysed our results and highlighted their accuracy and similarity with the reconstructions provided by the imaging station considered as reference. They pointed out the continuity of the vessels, the absence of holes, the smooth surfaces and the presence of all the structures with their bifurcations. The dimensions of the vessels showed a quite good correspondence and no over-segmentation was observed. The experts also noticed that some small vessels which are not visible on the Xtravision reconstructions were well reconstructed by our method.

3.3 Quantitative validation

The quantitative validation of the segmentation results was difficult to address due to a lack of ground truth. This is because the manual delineation of the multiple vessels frontiers of the vascular network is tedious and time-consuming. Although the visual analysis of the segmentation quality was sufficient in the case of our application to reach the goal of extracting the navigation paths, a partial quantitative validation was performed on a vessel section to complete the evaluation. A vessel segment was manually segmented on a set of 50 slices by a neuroradiologist using the application Image Segmenter of Matlab and also using the automatic region-growing method. The degree of agreement between the two obtained results was evaluated using the Dice Coefficient. The calculated Dice Coefficient value for this vessel segment was of 0.96 and therefore shows a good agreement between the manual and the automatic segmentations.

3.4 Main structures separation

In this section, we present a preliminary result of vascular structures separation, applied on one dataset. It leads to a new 3D visualization where arteries, veins and nidus are displayed with three different colours as shown on Fig 5.(d). This is of great interest to help neuroradiologists to improve their understanding of the complex angioarchitecture of AVMs. To achieve this labelling, the nidus is removed

from the segmented image by applying a closing-opening morphological operation based on a spherical SE whose size must be adjusted by the user according to the size of the nidus. Fig 5.(a) shows the result of this approximate nidus detection on a 3DRA. Fig 5.(b) shows the whole network obtained after removing the previously detected nidus. One can see that the network is “broken" into two or more parts. The identification of the artery network and the veins is then performed by the analysis of the sizes of the connected components. The arterial network which is the bigger structure connected to the ICA appears in red and the draining vein appears in blue on Fig 5.(c). Finally, the nidus is accurately recovered by subtracting the arterial and venous networks from the initial segmented object (Fig 5.(d)).

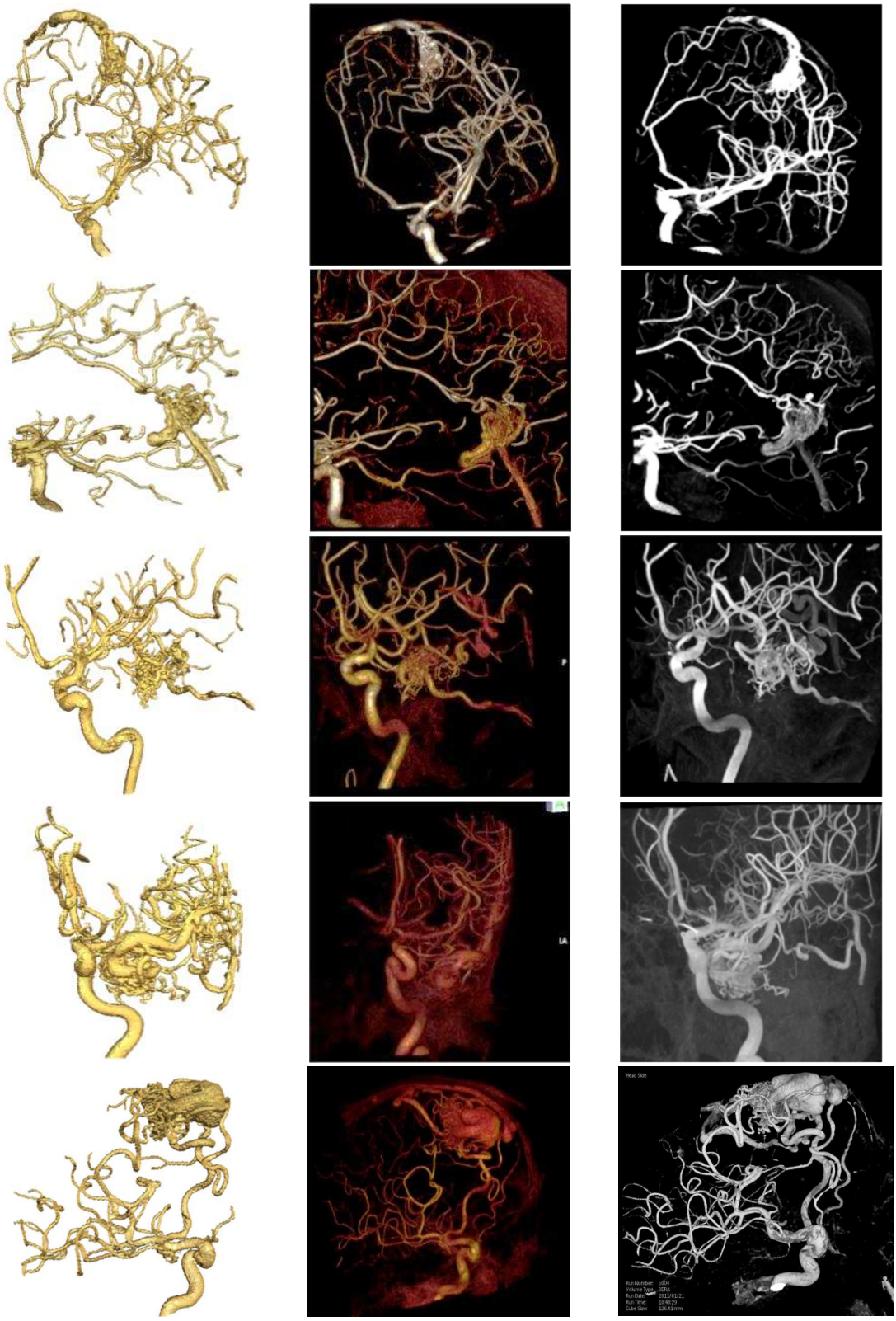

(a) (b) (c)

Fig 4. Comparison of the segmentation results obtained on clinical data, each row corresponding to a different patient. a) Visualization with the AMIRA 3D software of the segmentation results obtained by our method, b) volume rendering and c) 3D MIP rendering of the original 3DRA images visualized using the Osirix open-source software.

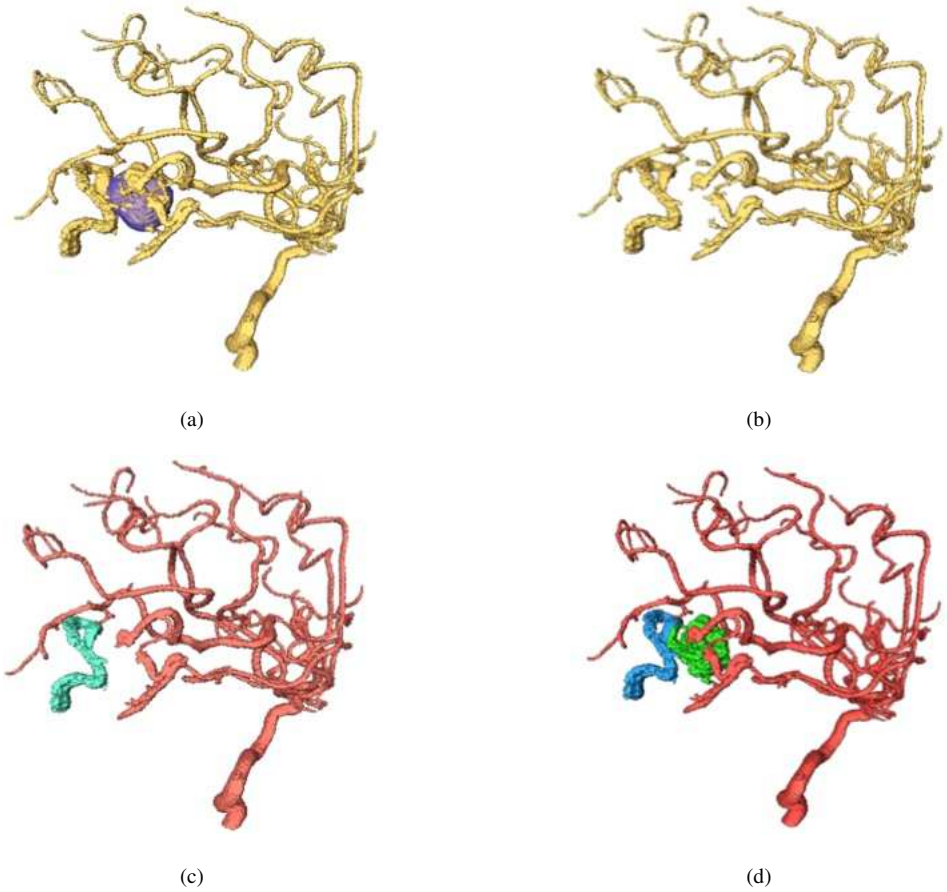

(a) (b)

(c) (d)

Fig 5. Separation of the three vascular components: arterial tree, veins and nidus; a) detection of the approximate shape of nidus, b) vascular network after removing the nidus, c) identification of the artery network and the veins and d) accurate extraction of the nidus and display of the three structures with different colours (arteries in red, veins in blue and nidus in green).

3.5 Symbolic representation and embolization paths determination

The symbolic representation of the vascular tree results from three successive steps that are displayed on Figure 6. The skeleton (Fig 6.(b)) is derived from the segmented vessels (Fig 6.(a)), using a thinning algorithm. Then, the skeleton points are classified in order to identify junctions and vessel segments (Fig 6.(c)). Fig 6.(d) illustrates the mathematical 2D graph that represents the hierarchical structure of the vascular network.

This representation gives the user the opportunity to select vascular sub-trees by determining a starting and an ending point. The corresponding path is then extracted and its features can be displayed. It is also possible to select a starting point and to specify a depth value that corresponds to Strahler number assigned to each branch.

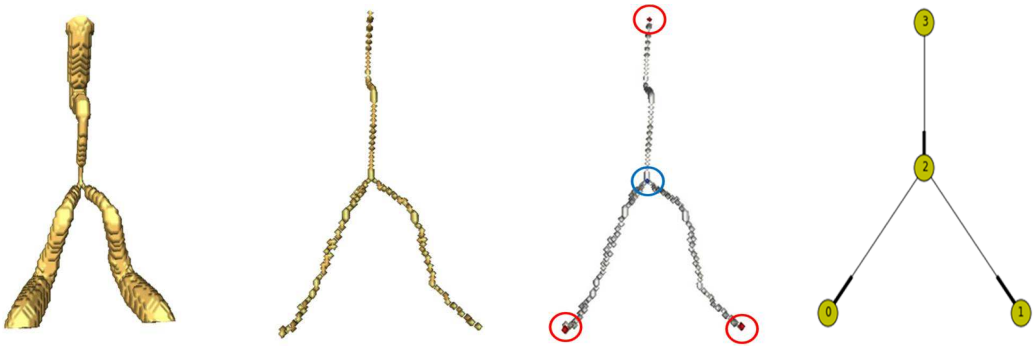

(a) (b) (c) (d)

Fig 6. A two-way graph-based vascular network representation: a) segmented vessels, b) their skeleton, c) skeleton point's classification, and d) 2D graph representation.

Thanks to this hierarchical model, we provide on the one hand selective visualizations of vascular sub-trees and on the other hand, a simple and objective access to the topology of the vascular network. Both are a valuable tool for surgical planning and catheterization procedures.

Results on synthetic images

The symbolic representation was first validated on a synthetic vascular network, generated by the VascuSynth open-source software [41], [42]. An illustration of the obtained results is given by Figure 7. The extracted centerlines of the synthetic vessels (Fig 7.(a)) present a rather curvilinear and smooth overall appearance (Fig 7.(b)). Different skeleton parts, such as end points, junctions and segments, were extracted. This gives an overview of the connectivity of the distribution of the vessels and the hierarchy of the vascular network. The associated graphs were then constructed in 3D on Fig 7.(c) and 2D on Fig.7.(d). In the 3D graph, the position of junction points and the length of vessels are kept in order to get a representation of the network closed to the real one whereas the 2D graph is a more conceptual classical binary tree structure with nodes corresponding to junction points and vessels to branches. We have also applied the Strahler model on the 2D graph, which permits a more clear demonstration of the parent-children relations.

By seeking for the graph-related edge of each segmented voxel, we decompose the vascular network into branches. Therefore each branch is extracted and separated from the vascular tree. The branch decomposition is shown on Figs 7.(e) and 7.(f). Each vessel branch is displayed by a user-defined colour. Visually, the mapping reveals a good agreement with the ground truth. In Fig 7.(g), all the terminal

branches (level 1) are displayed with blue, while the main branches were shown in green (level 2) and red (level 3). Figs 7.(h) and 7.(i) show the obtained navigation paths from the root (junction 6) to two different terminal points (respectively junctions 8 and 10). For a directed graph, the path from one depart point to an arrival point is unique.

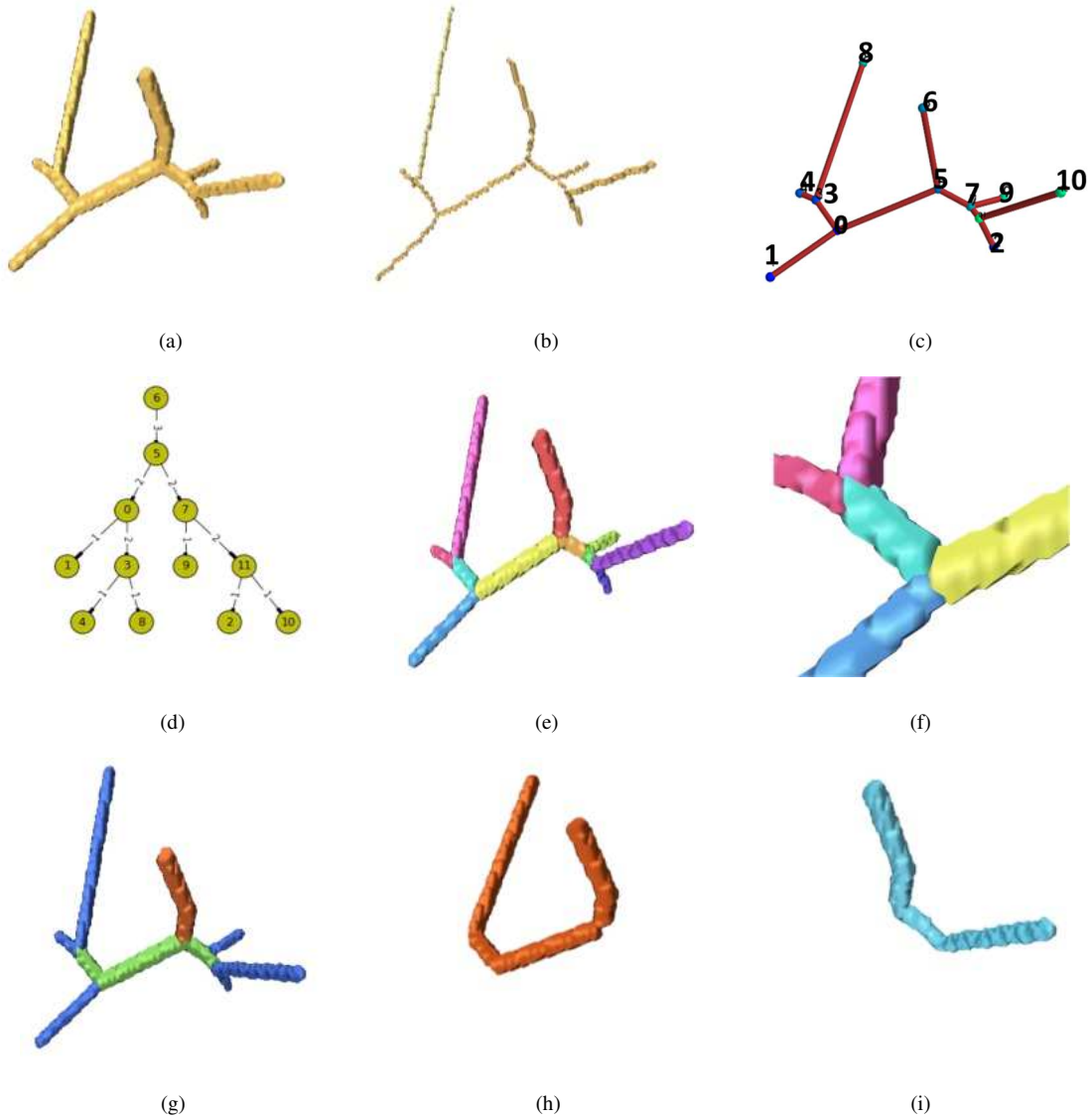

(a) (b) (c)

(d) (e) (f)

(g) (h) (i)

Fig 7. The symbolic representation results obtained on a synthetic vascular tree: a) synthetic vascular tree, b) curvilinear skeleton with Isthmus-based thinning, c) 3D graph representation of the vascular tree, d) 2D graph representation with Strahler level, e) branches decomposition, f) decomposition in bifurcations position, g) vascular tree colour representation of the Strahler orders, h) navigation path from junction 6 to 8 and i) navigation path from junction 6 to 10.

Results on clinical data

The symbolic representation procedure was carried out on a 3DRA dataset. The Figure 8 illustrates the complete process to get a selective visualization of vascular sub-trees. The Fig 8.(a) shows the initial MIP display provided by the 3DRA imaging device. The obtained result after our 3D vascular network segmentation is shown on Fig 8.(b) with a superimposed rectangle that defines a sub-tree to modelize (Fig 8.(c)). The following figures (Fig 8 .(d, e and f)) respectively correspond to the three steps described above for the synthetic images: skeletonization, 3D graphic representation and labelling of the segmented vascular tree. Finally, Figures 8 .(g, h and i) shows three different navigation paths providing by our model. As we can see, our model is really relevant and its ability to define paths in complex vascular networks is a breakthrough to assist neuroradiologists for endovascular navigation.

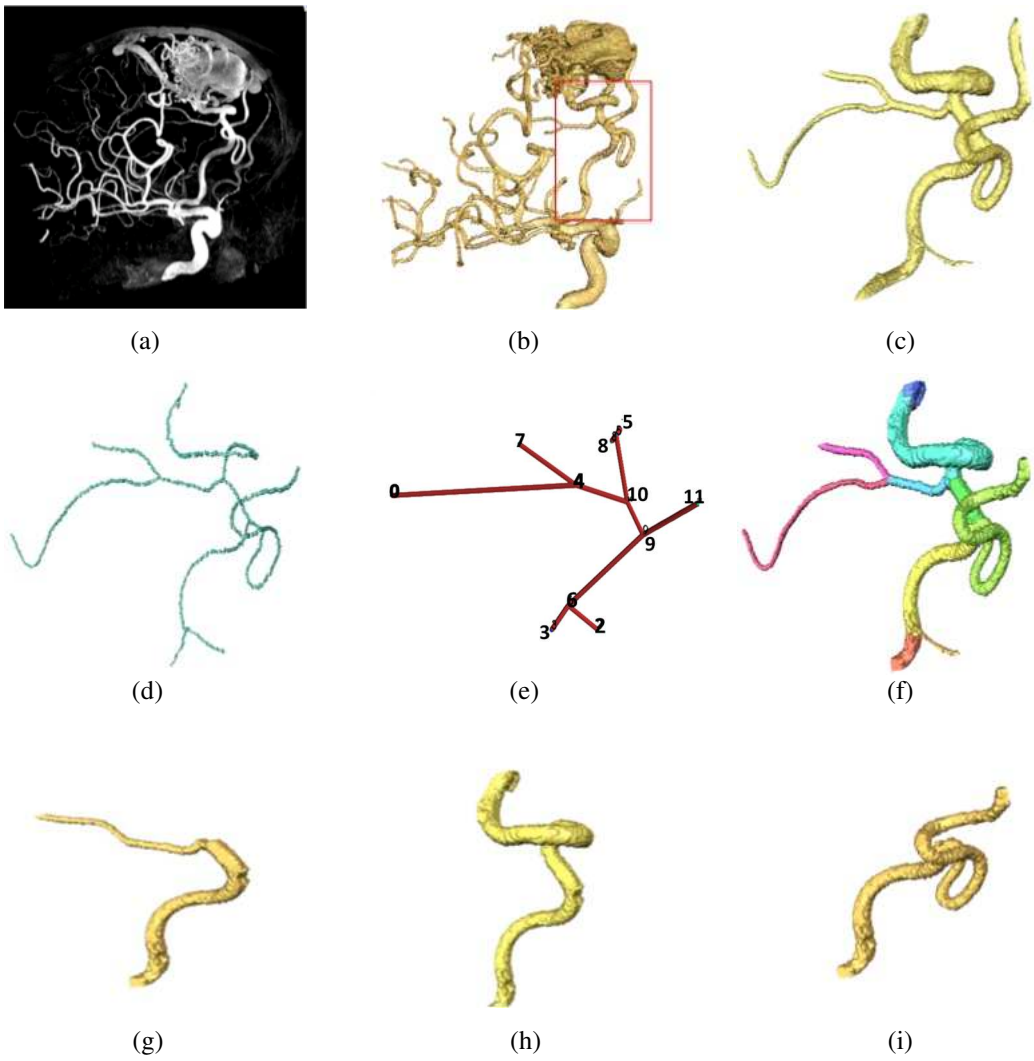

(a) (b) (c)

(d) (e) (f)

(g) (h) (i)

Fig 8. Selective visualization of vascular tree: a) a MIP image of the vascular network, b) the resulted 3D segmentation using the region-growing-based method, c) a sub-tree connected to the nidus, d) skeleton of the sub-tree, e) 3D graph of the sub-tree, f) decomposition into vessel branches and g), h), and i) three paths of the nidus supplying arteries.

To estimate the good agreement of our 3D visualization with the original MIP image, Figure 9 shows the image obtained by superimposing the extracted vessels on the 3D MIP image. We can see on Fig 9.(a) the vessel tree decomposition with the graph-based approach. Fig 9.(b) gives the same view with transparency. Finally, on Fig 9.(c), we can see in yellow the trajectory or the principle feeding artery of the nidus. It highlights a very good matching.

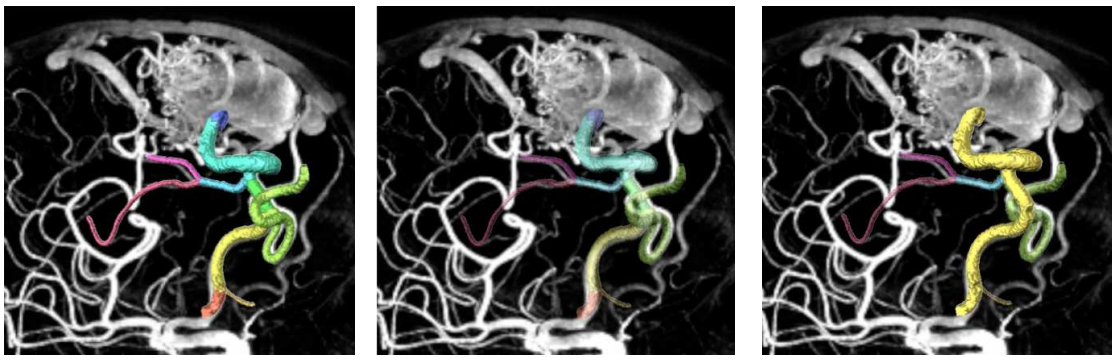

(a) (b) (c)

Fig 9. a) Overlay of MIP original image with the labelled vascular sub-tree, b) same result with transparency and c) the path of the principle feeding artery toward the nidus (in yellow).

The proposed segmentation algorithm was implemented using Matlab on the desktop computer with 2.4 GHz Intel Core 2 Duo processor with 8 GB of internal memory. The 3D segmentation step for one patient takes around 1 minute. For the structures separation, the operation on itself is instant; however it requires few tests to choose the suitable size of the structuring element (about 3 or four minutes). The proposed symbolic representation method was implemented with Python. The processing time of the whole procedure depends on the image size, resolution and number of branches of the vascular network. As an example, on the desktop computer with two cores 2.4 GHz processors, 8 GB internal memory, for one clinical image it takes around 1 hour. For a synthetic image, it takes approximately 15 minutes.

4. DISCUSSION

Few works have been devoted to cerebral vascular structures segmentation on 3DRA images and even less to the cerebral AVM network modelization [9], [15], [43]–[45]. Until now, there is no standard method for this kind of application and most proposed methods require user interaction [43]–[45]. Furthermore, pattern recognition, model-based or tube-like methods fail to segment the nidus and the malformed vessels whose complex shapes cannot be considered as cylinders. As 3DRA images present a good and uniform contrast between vascular structures and background, thanks to their high contrast resolution [32], the region-growing-based segmentation algorithm with an intensity-based evolution criterion represents an appropriate approach for this modality. This algorithm is simple to implement in a 3D manner and does not necessitate shape prior knowledge. In addition, 3DRA images avoid some problems such as lack of signal inside the vessels in MRI, which causes disconnections in the vascular structures or partial volume effects with X-ray tomography resulting in artefactual connections with the anatomical structures surrounding the vessels. Furthermore, separating the nidus from the arteries and veins represents a significant achievement since it brings a better visualization and comprehension of the complex architecture of the vessels. However, it needs some user interaction as multiple tests are required to find the appropriate size of the spherical SE used in the processing. A visual analysis of the obtained result for different SE sizes is essential to finally choose the most appropriate value. The symbolic representation of the vessels completes the process and provides the possibility to define the arterial supplies of the nidus by automatically extraction the paths and this is an important breakthrough in the assistance of neuroradiologists for interventional planning. However, this step must be improved to reduce the execution time. To conclude, if we compare our work to the existing techniques of 3D vascular segmentation or/and modelization, our developed pipeline has the advantage of being more complete by offering in addition solutions which could help in determining optimal paths for AVM embolization and also visually separating the different structures. In this context and to our knowledge, this work fulfils a real need and makes a significant contribution to the field.

5. CONCLUSION

This work aims to bring assistance to neuroradiologists in the perception, the interpretation and the exploitation of the 3DRA images for the planning of cerebral AVMs embolization interventions. Our contribution consists in the development of an innovative image processing pipeline, constituted by a dedicated 3D region-growing-based segmentation algorithm, and by a symbolic representation of the extracted vessels. Until now, few works carried out works to segment and modelize the complex AVMs vascular network from 3DRA imaging.

The segmentation process is automatically initialized and results in the extraction of the whole vascular network from the 3DRA images. This is a significant contribution that allows a better three-dimensional visualization of complex cerebral networks with AVM. The symbolic representation of the vessels establishes a link between the segmented image, the skeleton and the 3D graph, improving the understanding of the vascular network organization. The whole vascular tree is decomposed into single vessel branches. The topological relations provided by the 3D graph representation offer the possibility to isolate a part of the vascular network or to interactively select a single vessel. Thanks to this symbolic representation, a tangled network can be interpreted through a hierarchical model that reveals its topological structure. This is a precious tool to understand the complex angioarchitecture of the AVM vascularization and consequently to assist neuroradiologists in preoperative planning. Above all it allows easily determining embolization paths by selecting one or two points of the network.

Another significant contribution of this work is the ability to visualize separately the three principal structures which are the feeding arteries, the draining veins and the nidus. A visualization labelled with different colours even more improves the understanding of angioarchitecture. The developed algorithms have to be integrated into a user-friendly graphical interface, functional in clinical routine to assist the preoperative interventions planning and possibly the perioperative navigation. The malformations being very complex and different from a patient to another, this work could be applied on an enlarged database to confirm its efficiency and to assess its relevance in a clinical context. In future works, we aim to add to our model biomechanical measurements such as intravascular blood pressure and blood flow velocities.

Acknowledgements

Authors would like to acknowledge the ESME Sudria engineering school for funding this study and Doctor Hocine Redjem (HR) from Fondation Ophtalmologique Adolphe de Rothschild for his clinical validation of our results.

Conflict of interest

None Declared.

Summary

Endovascular embolization is a minimally invasive interventional method for the treatment of neurovascular pathologies such as aneurysms, arterial stenosis or arteriovenous malformations (AVMs). In this context, neuroradiologists need efficient tools for interventional planning and microcatheter embolization procedures optimization. Thus, the development of helpful methods is necessary to solve this challenging issue. This work aims to bring assistance to neuroradiologists in the perception, the interpretation and the exploitation of 3D rotational angiography (3DRA) images for the planning of cerebral AVMs embolization interventions. Our contribution consists in the development of an innovative image processing pipeline, constituted by a dedicated 3D region-growing-based segmentation algorithm, and by a symbolic representation of the extracted vessels. Until now, few authors carried out works to segment and modelize the complex AVMs vascular network from 3DRA imaging.

The segmentation step is automated and allows the extraction of the nidus and its feeding arteries and draining veins. The proposed algorithm presents the advantage of being automatically initialized. It's able to automatically segment a given vascular tree with all its branches. Specific forms like malformed vessels and junctions are automatically managed. Moreover, the process depends on few parameters whose values adapt according to the image properties even for the detection of complex vascular structures. A symbolic representation of the topologically related vessels is then built from the segmentation result. It's carried out in three steps: skeletonization, 2D and 3D graph-like representation and labelling of the vessels. This representation provides a vascular network modelization with hierarchical and geometrical features that brings a better comprehension of the complex vessels angioarchitecture. It also permits the determination, in the course of interventions planning, of the optimal paths for AVM embolization.

The 3D vascular tree segmentation was performed on ten 3DRA datasets with AVMs. A qualitative validation of the segmentation results was independently performed by two neuroradiologists and consisted of a visual comparison with volume rendering and 3D MIP rendering obtained with the Xtravision Unit imaging station. A preliminary result for the vascular structures separation is given for a 3DRA dataset and the symbolic representation result is validated on a synthetic vascular network.

In conclusion a relevant vascular network modelization has been developed that constitutes a breakthrough in the assistance of neuroradiologists for AVM endovascular embolization planning.

References

[1] Ondra SL, Troupp H, George ED, Schwab K., "The natural history of symptomatic arteriovenous malformations of the brain: a 24-year follow-up assessment," pp. 387–91, 1990.

[2] R. Blanc *et al.*, "Multimodal angiographic assessment of cerebral arteriovenous malformations: a pilot study," *J. NeuroInterventional Surg.*, vol. 7, no. 11, pp. 841–847, Nov. 2015.

[3] C. S. Ogilvy *et al.*, "Recommendations for the Management of Intracranial Arteriovenous Malformations: A Statement for Healthcare Professionals From a Special Writing Group of the Stroke Council, American Stroke Association," *Stroke*, vol. 32, no. 6, pp. 1458–1471, Jun. 2001.

[4] S. Bash *et al.*, "Intracranial vascular stenosis and occlusive disease: evaluation with CT angiography, MR angiography, and digital subtraction angiography," *AJNR Am. J. Neuroradiol.*, vol. 26, no. 5, pp. 1012–1021, May 2005.

[5] C. Kirbas and F. Quek, "A review of vessel extraction techniques and algorithms," *ACM Comput. Surv.*, vol. 36, no. 2, pp. 81–121, Jun. 2004.

[6] D. Lesage, E. D. Angelini, I. Bloch, and G. Funka-Lea, "A review of 3D vessel lumen segmentation techniques: models, features and extraction schemes," *Med. Image Anal.*, vol. 13, no. 6, pp. 819–845, Dec. 2009.

[7] K. Krissian, G. Malandain, N. Ayache, R. Vaillant, and Y. Trousset, "Model-Based Detection of Tubular Structures in 3D Images," *Comput. Vis. Image Underst.*, vol. 80, no. 2, pp. 130–171, Nov. 2000.

[8] Y. Sato *et al.*, "Three-dimensional multi-scale line filter for segmentation and visualization of curvilinear structures in medical images," *Med. Image Anal.*, vol. 2, no. 2, pp. 143–168, Jun. 1998.

[9] R. Gan, W. C. K. Wong, and A. C. S. Chung, "Statistical cerebrovascular segmentation in three-dimensional rotational angiography based on maximum intensity projections," *Med. Phys.*, vol. 32, no. 9, pp. 3017–3028, Sep. 2005.

[10] A. C. S. Chung, J. A. Noble, and P. Summers, "Vascular Segmentation of Phase Contrast Magnetic Resonance Angiograms Based on Statistical Mixture Modeling and Local Phase Coherence," *IEEE Trans. Med. Imaging*, vol. 23, no. 12, pp. 1490–1507, Dec. 2004.

[11] X. Gao, Y. Uchiyama, X. Zhou, T. Hara, T. Asano, and H. Fujita, "A fast and fully automatic method for cerebrovascular segmentation on time-of-flight (TOF) MRA image," *J. Digit. Imaging*, vol. 24, no. 4, pp. 609–625, Aug. 2011.

[12] B. Zhang, Z. Xing, J. He, S. Yi, and L. Ma, "Local optimal threshold segmentation and reconstruction of cerebrovascular MRA images," in *2012 5th International Conference on BioMedical Engineering and Informatics*, 2012, pp. 300–303.

[13] R. Wang *et al.*, "Threshold segmentation algorithm for automatic extraction of cerebral vessels from brain magnetic resonance angiography images," *J. Neurosci. Methods*, vol. 241, pp. 30–36, Feb. 2015.

[14] M. Boegel, P. Hoelter, T. Redel, A. Maier, J. Hornegger, and A. Doerfler, "A fully-automatic locally adaptive thresholding algorithm for blood vessel segmentation in 3D digital subtraction angiography," in *2015 37th Annual International Conference of the IEEE Engineering in Medicine and Biology Society (EMBC)*, 2015, pp. 2006–2009.

[15] L. Verscheure *et al.*, "Three-dimensional skeletonization and symbolic description in vascular imaging: preliminary results," *Int. J. Comput. Assist. Radiol. Surg.*, vol. 8, no. 2, pp. 233–246, Mar. 2013.

[16] E. Bullitt *et al.*, "3D Graph Description of the Intracerebral Vasculature from Segmented MRA and Tests of Accuracy by Comparison with X-ray Angiograms," in *Information Processing in Medical Imaging*, Springer, Berlin, Heidelberg, 1999, pp. 308–321.

[17] D. Babin *et al.*, "Generalized pixel profiling and comparative segmentation with application to arteriovenous malformation segmentation," *Med. Image Anal.*, vol. 16, no. 5, pp. 991–1002, Jul. 2012.

[18] A. Plaza, P. Martinez, R. Perez, and J. Plaza, "A new approach to mixed pixel classification of hyperspectral imagery based on extended morphological profiles," *Pattern Recognit.*, vol. 37, no. 6, pp. 1097–1116, Jun. 2004.

[19] D. Babin *et al.*, "Skeletonization method for vessel delineation of arteriovenous malformation," *Comput. Biol. Med.*, vol. 93, pp. 93–105, Feb. 2018.

[20] C.-Y. Hsu, M. Ghaffari, A. Alaraj, M. Flannery, X. J. Zhou, and A. Linninger, "Gap-free Segmentation of Vascular Networks with Automatic Image Processing Pipeline," *Comput Biol Med*, vol. 82, no. C, pp. 29–39, Mar. 2017.

[21] A. Danilov, Y. Ivanov, R. Pryamonosov, and Y. Vassilevski, “Methods of graph network reconstruction in personalized medicine,” *Int. J. Numer. Methods Biomed. Eng.*, vol. 32, no. 8, p. e02754, 2016.
[22] F. Li, O. Tankyevych, Y. Chenoune, R. Blanc, and E. Petit, “Symbolic Representation of Brain Vascular Network with ArterioVenous Malformations from 3DRA Images,” 37th Annual International Conference of the IEEE Engineering in Medicine and Biology Society (EMBC), pp. 662–665, 2015.
[23] E. Bullitt, S. Aylward, E. J. Bernard, and G. Gerig, “Computer-assisted visualization of arteriovenous malformations on the home personal computer,” *Neurosurgery*, vol. 48, no. 3, pp. 576–582; discussion 582-583, Mar. 2001.
[24] M. Graß *et al.*, “A method for 3D flow determination based on X-ray rotational angiography,” *Int. Congr. Ser.*, vol. 1230, pp. 408–414, Jun. 2001.
[25] A. Sankowski and A. Materka, “Mathematical morphology analysis of 3D MRA images of human brain for estimation of blood vessels parameters,” in *2012 Joint Conference New Trends In Audio Video And Signal Processing: Algorithms, Architectures, Arrangements And Applications (NTAV/SPA)*, 2012, pp. 49–52.
[26] M. Piccinelli, A. Veneziani, D. A. Steinman, A. Remuzzi, and L. Antiga, “A framework for geometric analysis of vascular structures: application to cerebral aneurysms,” *IEEE Trans. Med. Imaging*, vol. 28, no. 8, pp. 1141–1155, Aug. 2009.
[27] P. Orlowski *et al.*, “An approach to the symbolic representation of brain arteriovenous malformations for management and treatment planning,” *Neuroradiology*, vol. 56, no. 3, pp. 195–209, Mar. 2014.
[28] L. Vincent, “Morphological grayscale reconstruction in image analysis: applications and efficient algorithms,” *IEEE Trans. Image Process.*, vol. 2, no. 2, pp. 176–201, Apr. 1993.
[29] H.-H. Chang, G. R. Duckwiler, D. J. Valentine, and W. C. Chu, “Computer-assisted extraction of intracranial aneurysms on 3D rotational angiograms for computational fluid dynamics modeling,” *Med. Phys.*, vol. 36, no. 12, pp. 5612–5621, Dec. 2009.
[30] F. Li, Y. Chenoune, M. Ouenniche, R. Blanc, and E. Petit, “Segmentation and reconstruction of cerebral vessels from 3D rotational angiography for AVM embolization planning,” *Conf. Proc. Annu. Int. Conf. IEEE Eng. Med. Biol. Soc. IEEE Eng. Med. Biol. Soc. Annu. Conf.*, vol. 2014, pp. 5522–5525, 2014.
[31] R. Jain, R. Kasturi, and B. G. Schunck, *Machine Vision*. Indo American Books, 2016.
[32] M. Schaap *et al.*, “Coronary lumen segmentation using graph cuts and robust kernel regression,” *Inf. Process. Med. Imaging Proc. Conf.*, vol. 21, pp. 528–539, 2009.
[33] N. D. Forkert, T. Illies, E. Goebell, J. Fiehler, D. Säring, and H. Handels, “Computer-aided nidus segmentation and angiographic characterization of arteriovenous malformations,” *Int. J. Comput. Assist. Radiol. Surg.*, vol. 8, no. 5, pp. 775–786, Sep. 2013.
[34] N. D. Forkert *et al.*, “3D cerebrovascular segmentation combining fuzzy vessel enhancement and level-sets with anisotropic energy weights,” *Magn. Reson. Imaging*, vol. 31, no. 2, pp. 262–271, Feb. 2013.
[35] F. Clarençon *et al.*, “Elaboration of a semi-automated algorithm for brain arteriovenous malformation segmentation: initial results,” *Eur. Radiol.*, vol. 25, no. 2, pp. 436–443, Feb. 2015.
[36] M. Couprie and G. Bertrand, “Asymmetric parallel 3D thinning scheme and algorithms based on isthmuses,” *Pattern Recognit. Lett.*, vol. 76, pp. 22–31, Jun. 2016.
[37] Z. Aktouf, G. Bertrand, and L. Perroton, “A three-dimensional holes closing algorithm,” *Pattern Recognit. Lett.*, vol. 23, no. 1, pp. 523–531, 2002.
[38] G. Bertrand and G. Malandain, “A new characterization of three-dimensional simple points,” *Pattern Recognit. Lett.*, vol. 15, no. 2, pp. 169–175, Feb. 1994.
[39] “Quantitative analysis of watershed geomorphology - Strahler - 1957 - Eos, Transactions American Geophysical Union - Wiley Online Library.” [Online]. Available: https://agupubs.onlinelibrary.wiley.com/doi/abs/10.1029/TR038i006p00913. [Accessed: 04-Jun-2018].
[40] H. Bogunović *et al.*, “Automated landmarking and geometric characterization of the carotid siphon,” *Med. Image Anal.*, vol. 16, no. 4, pp. 889–903, May 2012.
[41] P. Jassi and G. Hamarneh, “VascuSynth: Vascular Tree Synthesis Software,” p. 12.
[42] G. Hamarneh and P. Jassi, “VascuSynth: Simulating vascular trees for generating volumetric image data with ground-truth segmentation and tree analysis,” *Comput. Med. Imaging Graph.*, vol. 34, no. 8, pp. 605–616, Dec. 2010.

[43] Y. Kumar, “Vascular Segmentation of Cerebral AVM,” *Adv. Res.*, vol. 2, no. 1, pp. 52–57, Jan. 2014.
[44] R. P. Kumar, F. Albregtsen, M. Reimers, B. Edwin, T. Langø, and O. J. Elle, “Blood Vessel Segmentation and Centerline Tracking Using Local Structure Analysis,” in *6th European Conference of the International Federation for Medical and Biological Engineering*, Springer, Cham, 2015, pp. 122–125.
[45] M.-O. Berger, R. Anxionnat, E. Kerrien, L. Picard, and M. Söderman, “A methodology for validating a 3D imaging modality for brain AVM delineation: application to 3DRA,” *Comput. Med. Imaging Graph. Off. J. Comput. Med. Imaging Soc.*, vol. 32, no. 7, pp. 544–553, Oct. 2008.